Applied Materials Today 29 (2022) 101605

Contents lists available at ScienceDirect

Applied Materials Today

journal homepage: www.elsevier.com/locate/apmt

Layered graphene/hexagonal boron nitride nanosheets (Gr/*h*-BNNs) applied to the CO_2 photoconversion into methanol

Paulo V.R. Gomes [a], Nathalia F.B. Azeredo [a], Luis M.S. Garcia [a], Priscilla J. Zambiazi [a], Giovanni R. Morselli [b], Rômulo A. Ando [b], Larissa Otubo [a], Dolores R.R. Lazar [a], Rodrigo F.B. de Souza [a], Debora F. Rodrigues [c], Almir O. Neto [a,*]

[a] *Instituto de Pesquisas Energéticas e Nucleares, Av. Prof. Lineu Prestesn 2242, São Paulo CEP 05508-000, Brazil*
[b] *Laboratório de Espectroscopia Molecular, Departamento de Química Fundamental, Instituto de Química, Universidade Estadual de São Paulo – USP, Av. Prof. Lineu Prestes, 748, São Paulo CEP 05508-000, Brazil*
[c] *Department of Civil and Environmental Engineering, University of Houston, TX 77204-4003, United States*

ARTICLE INFO

Keywords:
Non-thermal plasma source
White graphene
Boron-doped
Hybrid nanofilms
CO_2 photoreduction

ABSTRACT

Photocatalysts based on heterostructure 2D materials show promising properties for the construction of optoelectronic devices for selective reduction of CO_2 to methanol. In this sense, a fast and simple method to produce 2D hexagonal hybrid BN nanosheets (*h*-BNNs) doped with graphene heterostructure by van der Waals interactions was developed. The method used plasma created by a Tesla coil. The Gr/*h*-BNNs hybrid material obtained presented a stacking structure containing *h*-BNNs and graphene layers. The structure included doping of carbon atoms along the *h*-BN edge structures. The doping of the *h*-BN nanostructure with graphene sheets, conferred adaptable optical properties to the semiconductor, resulting in band gap energy values favorable to photocatalysis. The reaction promoted selective reduction of CO_2 to methanol, and synthesis of other products, such as formaldehyde and formic acid, due to multielectronic transfer processes.

1. Introduction

Two-dimensional (2D) layered composites are promising candidates for many technological areas, such as energy, catalysis, electronics, and mechanics [1,2]. Graphene (Gr) is currently one of the most famous 2D materials, attracting intense experimental and theoretical research efforts since isolated by Novoselov. According to Yankowitz [3], the heterostructures of the graphene supports on with hexagonal boron nitride (hBN) open a new area in 2D materials research. Due to its electronic properties on hBN heterostructures, graphene may also be utilized to design novel devices, such as re-writable p-n junctions [4] and the mechanical propriety, structural reinforcement and thermal conductivity [5] that this composite has. However, obtaining this material is of a great challenge, mainly due to the difficulty in exfoliating hBN.

The 2D layered materials have good conductivity and superior electron mobility because of the presence of the 2D π-conjugated structure in graphene, providing an ultrafast electron transfer platform to facilitate the transfer and separation of photogenerated electrons and holes in the photocatalyst [6,7].

Photocatalysts based on 2D layered composite present unique properties, such as charge transport which are beneficial to enhance the photocatalytic performance, band gap tuning, and heterojunction formation [3,4]. In addition, the bond B-N in the hBN nanosheets (hBNNs) is an ionic structure, making the hBNNs more resistant to oxidation and to corrosion than the covalent C-C bond of graphene [8], increasing the durability of the material.

The 2D photocatalyst materials have emerged as promising candidates for traditional semiconductors. These catalysts usually possess shorter carrier diffusion pathways, higher specific surface areas and conductivity, more vacancy-type defects, and exposed edges when compared to their bulk counterparts [9].

Photocatalytic reduction of CO_2 in commercial products has attracted attention to the scientific community to mitigate excessive greenhouse gas emissions by mimicking the natural photosynthetic process [10,11]. Higher efficiency and product, as a methanol, formate, and others yield can be achieved by designing a suitable photocatalyst with retarded recombination of photogenerated electron-hole pairs and sufficient potential for the reduction of CO_2 [12]. This propriety is

* Corresponding author.
E-mail address: aolivei@usp.br (A.O. Neto).

https://doi.org/10.1016/j.apmt.2022.101605
Received 12 May 2022; Received in revised form 13 July 2022; Accepted 23 July 2022
Available online 28 July 2022

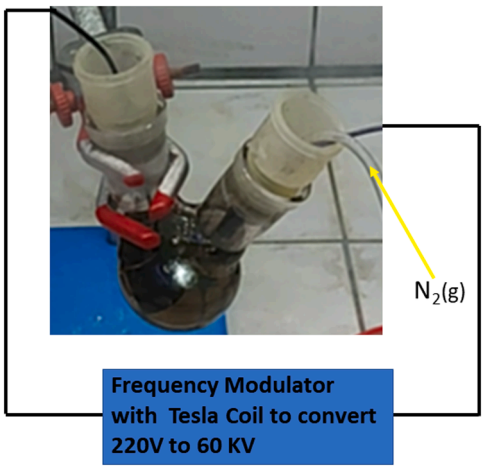

Fig. 1. Non-thermal plasma generator coupled to a reaction vessel with cyclohexane, nitride-BN and $N_{2(g)}$ flow for hybrid Gr/hBNNs nanofilm production.

beneficial for the separation of photogenerated carriers promoted by Gr/hBN materials, as well as for the adsorption and activation of CO_2 molecules [13].

In this sense, this work presents a clean, rapid and facile technique to synthesize graphene on *h*-BN during this nitride exfoliation by a Non-Thermal Plasma Source. The synthesized hybrid material exhibited optoelectronic properties due to the nanometer-scale spacing between the 2D layers. The photocatalytic reduction of CO_2 to more valuable compounds was also investigated, revealing very promising results in terms of efficiency.

2. Experimental

The hexagonal boron nitride nanosheets doped with graphene were synthetized in one step by an adapted non-thermal plasma method developed by Souza et al. [14] coupled to a reaction vessel (Fig. 1). In this reactor, using h-BN ~1 μm, 98% Aldrich and cyclohexane Aldrich in ratio of 1:400 m/m and input 60kV arc with $N_{2(g)}$ flow between a 316 L steel electrode and another one made of mineral graphite, until there was no more liquid. The material was then collected and washed in mixture 1:1 of water and isopropanol, and the solid was filtered on a cellulose acetate membrane with pores of 200 nm. The powder obtained was dried.

The dry material was characterized by transmission electron microscopy (TEM) using a JEOL JEM-2100 electron microscope, operated at 200 kV. The X-ray diffraction (XRD) were obtained using a diffractometer model Miniflex II, with Cu kα radiation source of 0.15406 Å, set at 2θ range 2–90°, with 2 min^{-1} scan speed, and the graphene load in h-BN matrix was determined using a Shimadzu Thermogravimetric analysis (TGA) 51H/TA-60WS. The Raman spectra was collected using Horiba Scientific MacroRam Raman spectroscopy equipment with laser 785nm. The Fourier transform infrared spectroscopy (FTIR) was performed on an attenuated total reflection (ATR) accessory (MIRacle with a ZnSe Crystal Plate Pike®) installed on a Nicolet® 6700 FTIR spectrometer equipped with a cooled MCT detector with N_2 liquid.

The optical properties were measured using a Shimadzu UV-Vis NIR UV-3101PC spectrometer with an integrating sphere module ISR-3100 to obtain the UV-Vis spectra by diffuse reflectance. The samples were dispersed in $BaSO_4$ cells, and the spectra were obtained in a configuration of slit width of 12 nm, in a range between 200-600 nm, and a collection interval of 0.5 nm.

The photocatalysis experiments were performed in a reactor presented by Yovanovich et al. [15], with a gas inlet for adapted gas diffusion layers, where a medium-pressure mercury (254 nm, 8 W) and xenon (65 W) lamp were used to provide UVC-visible and white light irradiation. The 10 mL min^{-1}dry $CO_{2(g)}$ flow passed through the carbon diffuser support, produced with 40 mg of carbon Vulcan (Cabot ®) and agglutinated with a 2% PTFE suspension (DuPont TM 30). The porous-thin layer of the photocatalyst was prepared by mixing the composite (20 mg) with 2% PTFE suspension (DuPont TM 30) for 1 h until the water interface was observed. The quantification of methanol was obtained by Boyaci's method with Raman spectroscopy [16,17]. The standard curve was constructed with methanol with a concentration range of 0.005-1.000 mol L^{-1}. The intensity of the methanol in the standard curve was 28.9115 + 84.1535[methanol] with a correlation coefficient of 0.945.

3. Results and discussion

The XRD pattern of the material obtained is presented in Fig. 2A in comparison with the h-BN starting powder. The diffraction peaks relative to the planes of the BN hexagonal phase (002), (100), (101), (102), (004), (110), and (112) were at 26.7°, 41.6°, 43.7°, 54.9°, 76°, and 82.2°, respectively (JCPDS card 34-0421). The (002) peak of the exfoliated BN presented a shift to ~ 0.1° less positive 2θ in comparison to the *h*-BN raw (Fig. 2B), according to the literature [14,18]. This result suggests the expansion of the interplanar distance for (002) and the exfoliation in the *c* direction.

In Fig. 2C, the XRD pattern was plotted on a logarithmic scale, to investigate the formation of graphene on h-BN material. According to the graphene crystallographic pattern, there is evidence of nanoflakes stacking and crystalline size in the graphene crystalline plane, and it can be observed in the (002) and (100) planes at 2θ ~ 22.6° and 25.1°, in addition to the corresponding plane h-BNNSs [19,20].

The Raman spectra of the composite and *h*-BN raw (Fig. 3A) showed the E_{2g} band of boron nitride at 1349 cm^{-1} for the raw material and 1351 cm^{-1} for the composite. The significant decrease in the intensities, resulting from the weaker interactions between the hBN layers due to the exfoliation, and is observed a blue shift of 2 cm^{-1} in this band, more one indicative of hBN exfoliation. In addiction the full width at half maximum (FWHM) of the E_{2g} band higher than reference material indicated the formation of hBNNs structure with few layers [21,22]. The graphene was identified in the bands D1 (1319 cm^{-1}), D2(1629 cm^{-1}), D3(1501 cm^{-1}), D4 (1202 cm^{-1}) and G (1593 cm^{-1}) [23] convoluted with the E_{2g} of *h*-BNNs. The intensity of the D-band higher than G-band suggests the graphene are nanoflakes [24] and the ratio of the ratio of I_{D1}/I_{D2} = ~ 6.4 indicated vacancies in the hexagonal structure [25].

The FTIR spectra shown in Fig. 3B revealed two main characteristic bands of h-BN at ~ 1370 cm^{-1} (E_{1u} mode) and ~ 817 cm^{-1} (A_{2u} mode) [26], which convoluted in the bands at ~1645 cm^{-1} (C=O) and at 1448 cm^{-1} (–OH) ascribed to the oxygen-containing functional groups presented on Gr/hBNNs [27]. It is commonly reported a band at ~3268 cm^{-1} for the *h*-BN exfoliated material, which corresponds to the hydroxyl group (-OH), that appear due to large amounts of defects, such as vacancies [28,29].

The XRD pattern indicated a low load of graphene on the h-BNNs substrate, and was confirmed by the ratio of the mass loss observed in the TGA analysis in function of the temperature. The TGA curve is used to describe the oxidative thermal stability of the material. Fig. 4 shows the mass-change (% initial mass) of the Gr/h-BNNs composite as a function of temperature. Initially, the TGA curve showed a small drop in mass, which can be attributed to loss of water molecules. From that point ahead, a more significant drop in mass was observed, with the combustion of graphene sheets in an oxidizing atmosphere, which occurred up to a temperature of approximately 650°C. Above this temperature, the mass was stable due to the presence of h-BN, which has been described in the literature to have thermal stability of up to 1000°C [30,31]. Based on the TGA results, the ration of 9:1 for was determined

The TEM images served to confirm the nanostructure properties of the Gr/h-BNNs hybrid material. Fig. 5A and B show the arrangement of

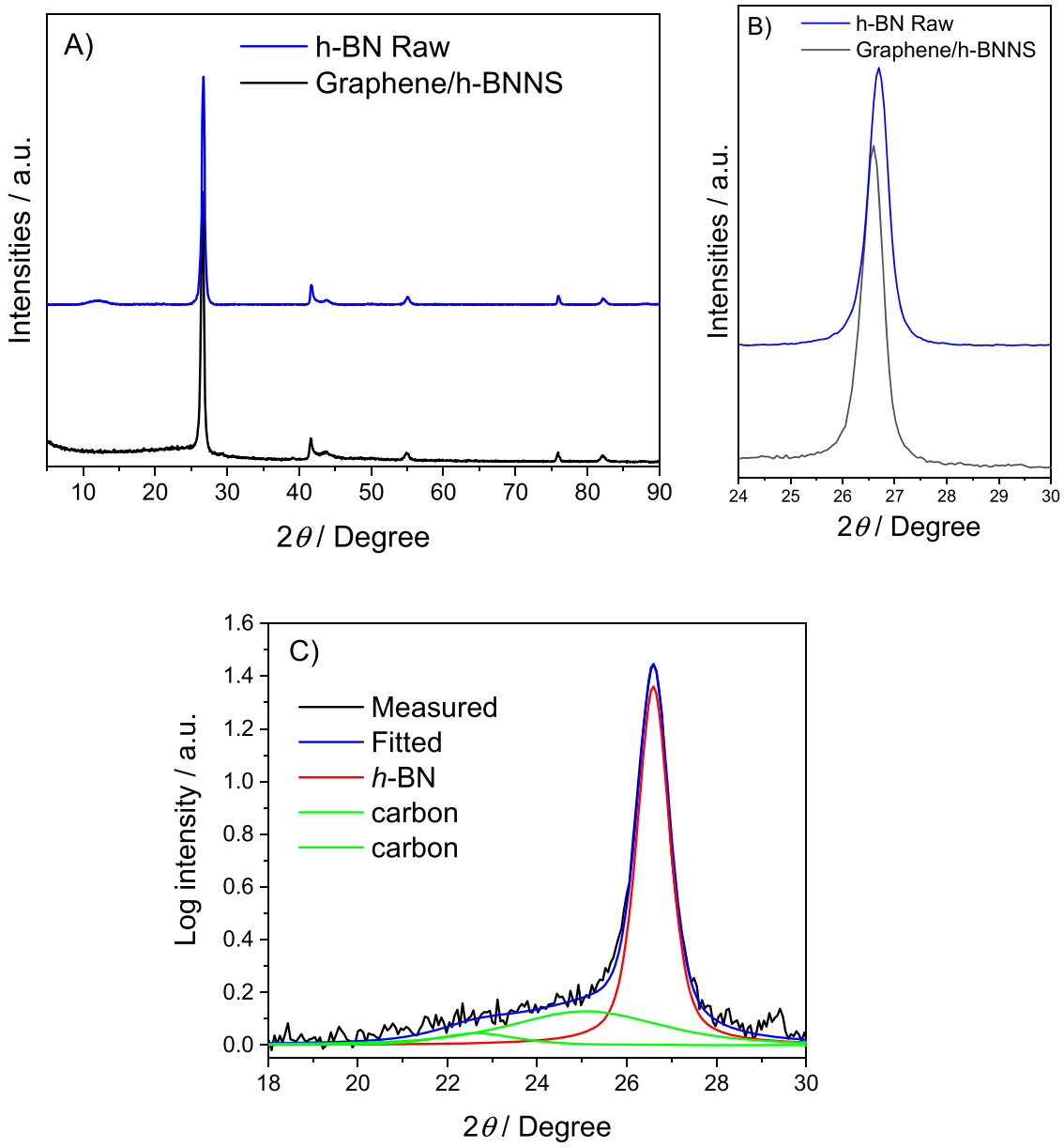

Fig. 2. (A) X-ray diffraction of the layered Gr/h-BNNs, (B) h-BN raw material peak (002), (C) detail of plane graphene (002) with deconvolution.

the material, revealing the homogeneity of its thin nanosheets *h*-BN and the graphene heterostructure. Furthermore, the material with nanocrystalline structure was formed from stacks of sheets (Fig. 5G). The *h*-BN and graphene nanosheets tend to stack alternately, resulting in a nanostructured hybrid material consisting of building blocks producing independent layers.

Fig. 5C presents the details of the material nanostructure. The high-resolution TEM images Fig. 5D showed the stacking of ultra-thin nanosheets forming mono- and/or multi-layer blocks. The FFT pattern indicates that these layers have a *d*-spacing of approximately 0.3463 nm relative to the crystallographic plane (002). The stacking of planar structures of *h*-BN and graphene, by van der Waals interactions, was characteristic in the hybrid structures of the Gr/h-BNNs [32,33]. Fig. 5E shows the stacking of approximately 21 layers, and from the FFT pattern, we confirmed the nanostructure presence of interplanar fringes with a distance between the atomic planes of 2.116 Å indicating a crystalline plane (001). The material heterostructure composition of self-assembled blocks by layers of *h*-BN and graphene (Fig. 5F) were stacked alternately in one direction. The FFT pattern shows stacked two-layers hexagonal lattices, where they have a rotational angle between them of about 19°. Furthermore, the structure of the hybrid solid extended laterally by bonds of the *h*-BN structure with the graphene, by the edge sewing.

The optical properties of the hybrid material were determined by diffuse reflectance UV-Vis spectroscopy analyses. In order to investigate the optical energy bandgap of the hybrid film, the Tauc plot was used to determine the band gap energy of the semiconductor [34]. Graphene has very weak absorption edges in the range of 200-800 nm, while *h*-BN has strong absorption at a wavelength of approximately 218 nm [35]. Carbon doping in boron nitride materials results in a composite with adjustable band gap energy. Fig. 6 shows the two absorption edges of the Gr/h-BNNs hybrid film. This result indicates the evidence of possible structures which was discussed earlier with the analyses of HR-TEM and XRD of the material.

Furthermore, these results were able to confirm that the hybrid material presented a self-assembling nanostructure in layers of *h*-BN and graphene. This structure contributed to the greater stability of the composite due to the formation of small polar interlayer bonds, and

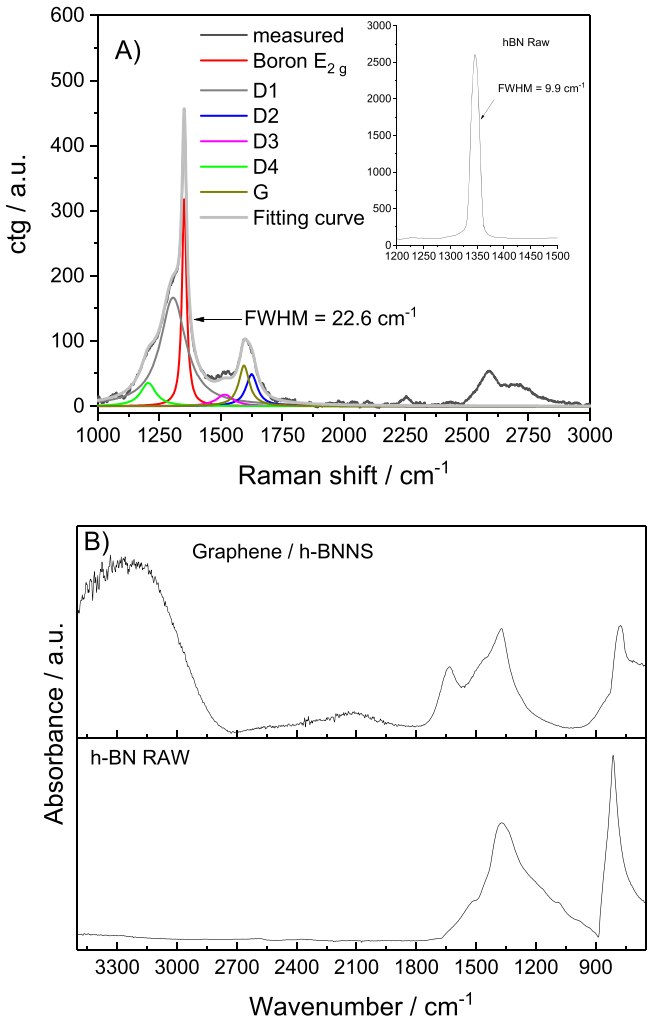

Fig. 3. (A) Raman and (B) FTIR spectra of BN raw and exfoliated BN.

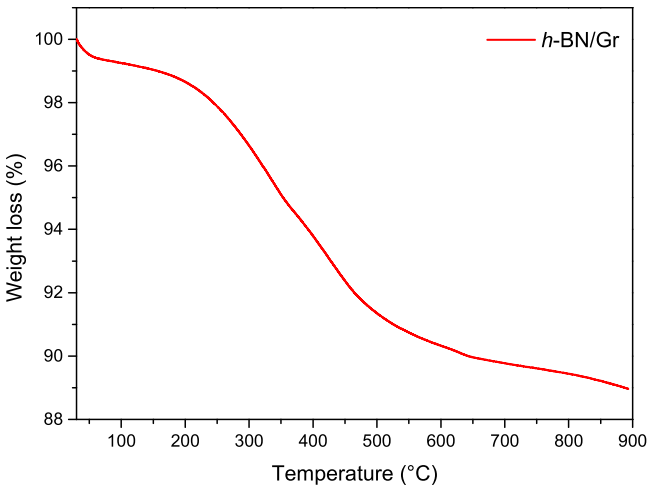

Fig. 4. The TGA graphic of the hybrid material Gr/h-BNNs in the temperature range of 30–900°C.

possible defects in the structure of *h*-BN containing the carbon atoms [19,20].

The first absorption edge refers to a band equal to 4.41 eV for the material with a ratio of 9:1 (Gr/h-BNNs). This optical energy is a result of carbon doping sp^2 in the *h*-BN framework domains. The second absorption edge has an optical band gap equal to 3.53 eV, and according to the TEM image, the size of the hybrid film structure is on the scale of a few nanometers. The heterostructure materials built in atomic layers show a change in their electronic structure, as is the case of the Gr/h-BNNs hybrid film presenting two optical band gap values. This characteristic gives the material promising semiconductor properties. Furthermore, the optical energy of the material indicates the edge effects of graphene on the *h*-BN structure, forming a superlattice, which may imply the formation of heterostructures by a physical stacking process, as observed in the powder diffraction pattern [36].

The activity of this composite for CO_2 conversion in methanol was evaluated by the immobilized catalyst in a thin porous layer on a carbon diffusion gas support with continuous dry CO_2 flow to the interface photocatalyst/water. During the photocatalytic experiments, an aliquot of aqueous solution was collected and analyzed by FTIR to identify the species formed. In Fig. 7, the FTIR spectra of aliquots of aqueous solution of products obtained during the 60 min for each radiation source, and observed the band centered at 1082 cm^{-1}, 1050 and 1030 cm^{-1} were attributed to methanol [16,37]. It was see band at 1267 cm^{-1} and 1172 cm^{-1} corresponding to formaldehyde [38], however, in UVC irradiation when the methanol bands decrease. The formic acid is also viewed at 1112 cm^{-1} [39].

The amount of methanol produced by photocalysis over Gr/hBNNs was shown in Fig. 8. This result depicts the yield of methanol obtained after 1 h of irradiation with UV and white light. After this time, 52μmol g^{-1} was obtained in visible light and a maximum of 47 μmol g^{-1} in 10 min with UVC light. As described by Karamian [40] the CO_2 adsorbed on the photocatalyst surface upon receiving a charge of on electron, forms the anionic radical $\cdot CO_2^-$, which in an environment rich in hydrogen species, such as water, can form methanol among other products (Fig. 8). The water is also activated by the photocatalyst where it provides hydrogen species. However, the high energy of the ultraviolet radiation also increases the production of ·OH species, and in excess, this species can degrade the products formed, returning to CO_2. Fig. 9 when the reaction is carried out under ultraviolet light is notable the decrease the methanol obtained after 10 min. The control experiment without the photocatalyst was performed and did not exhibit activity for this reaction.

The emerging nanomaterials formed by building blocks resulted in sets of light energy harvesting through their conductive properties, surface area and modified morphology. Hybrid film of Gr/h-BNNs constructed by van der Waals interactions gave birth to a material with high photocatalytic activity due to graphene doping on *h*-BN nanosheets. This photocatalytic enhancement was attributed to photogenerated electron-hole recombination, extended excitation wavelength, as a consequence of the increased reagents adsorption on the material surface. In this case, the Gr/h-BNNs hybrid material had optical properties that contributed to the promotion of active sites around the surface.

The two energy absorption edges observed in the Gr/h-BNNs were an effect of the carbon atoms dopant presence adjacent to the laminar structure of boron nitride. This structural feature of the hybrid film resulted in the modification of the band structure giving high photocatalytic performance to the semiconductor material, where energy levels were adjusted by chemical variations. In this case, the modification of the electronic band structure resulted in a new energy gap between the valence and conduction bands, promoting a transfer of electrons from the semiconductor material for the activation of CO_2 molecules generating CO_2^- species. Furthermore, the chemical reaction was promoted on the semiconductor surface selectively by electrons with reducing power, leading to the formation of methanol in the presence of H_2O, due to the selective oxidation capacity promoted by holes [32,41–43].

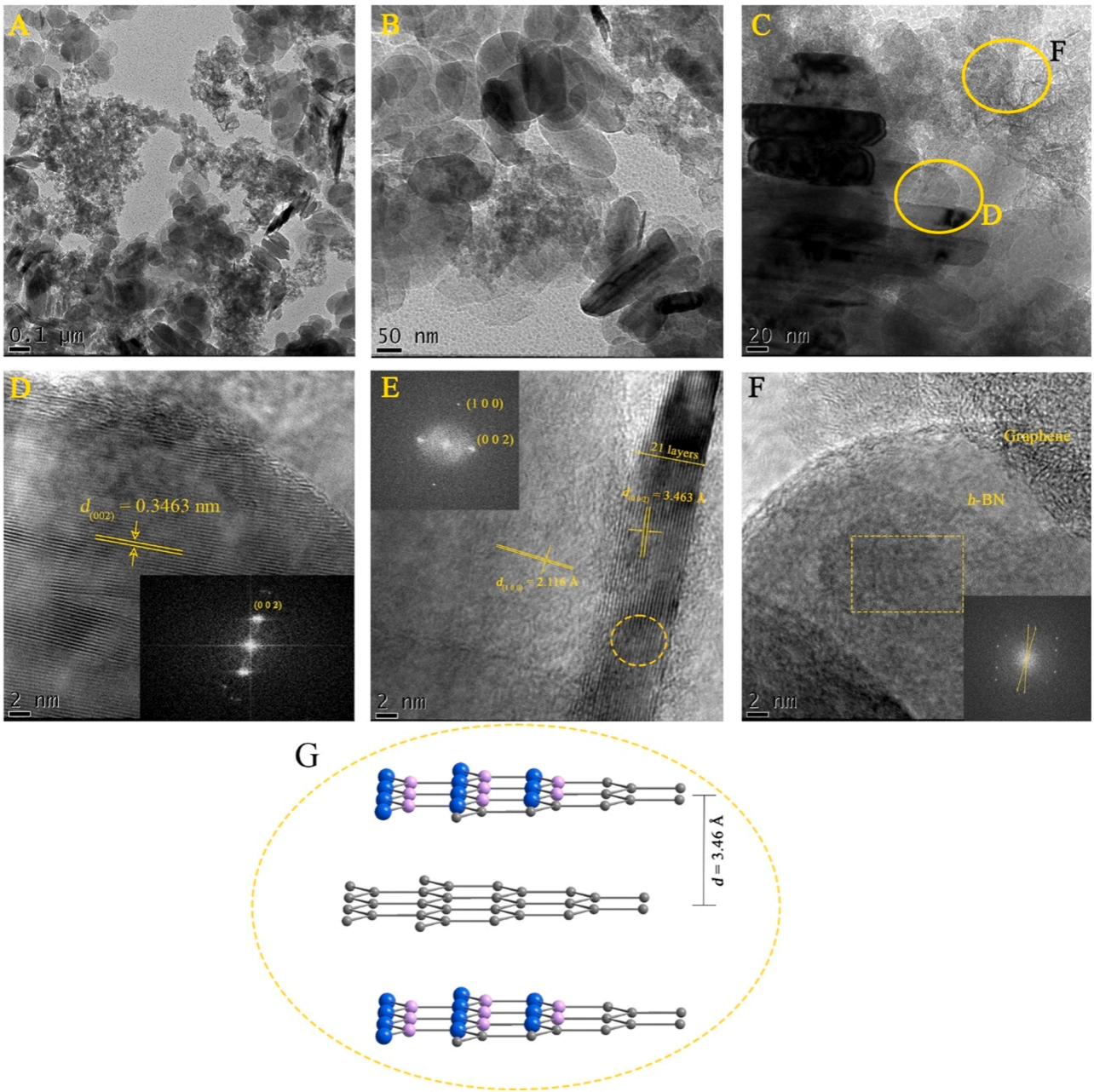

Fig. 5. TEM images of the hybrid material Gr/h-BNNs. (A, B and C) Homogeneity of thin nanosheets of *h*-BN and graphene; nanostructure details in 2 nm scale of the HR-TEM images in: (D) The edge of the *Gr/h-BNNs* layers with *d*-spacing about 0.346 nm and the FFT pattern of the (002) crystallography plane; (E) Stacking of 21 layers by van der Waals interactions and the FFT pattern of the crystalline planes (100) and (002), and (F) Films of *h*-BN and graphene, and the FFT in the inset reveal layers stacking with a rotational angle of about 19°. (G) Image of the nanostructure packing formed by the *h*-BN and Graphene layers include the carbon atom dopped in the *h*-BN structure.

4. Conclusion

This work presented the development of 2D heterostructural materials of boron nitride and graphene, based on a non-thermal plasma generator, a fast and accessible method for demands of mild conditions. The nanostructural properties of the hybrid nanofilm were determined by transmission imaging microscopy (TEM). The complementary XRD data showed the predominant h-BNNs pattern and low profile of graphene, this was in agreement with the TGA analysis. The hybrid formation of *h*-BN and graphene gave the material promising and adjustable optical properties, which were determined by diffuse reflectance UV-Vis spectroscopy analyses. The optical energy bandgap of the hybrid film was investigated using the Tauc plot to determine the band gap energy of semiconductors. The presence of two absorption edges of the material resulted in an energy gap between the valence and the conduction bands. A transfer of electrons from the semiconductor material promoted the activation of CO_2 molecules generating $CO_2^{\cdot-}$ species, a photocatalytic reduction of CO_2 to more valuable compounds such as methanol. The hybrid nanofilm Gr/h-BNNs showed that methanol production activity about 52 μmol g^{-1} in visible light and a maximum of 47 μmol g^{-1} in 10 min in UVC light.

The manuscript was written through contributions of all authors. All authors have given approval to the final version of the manuscript.

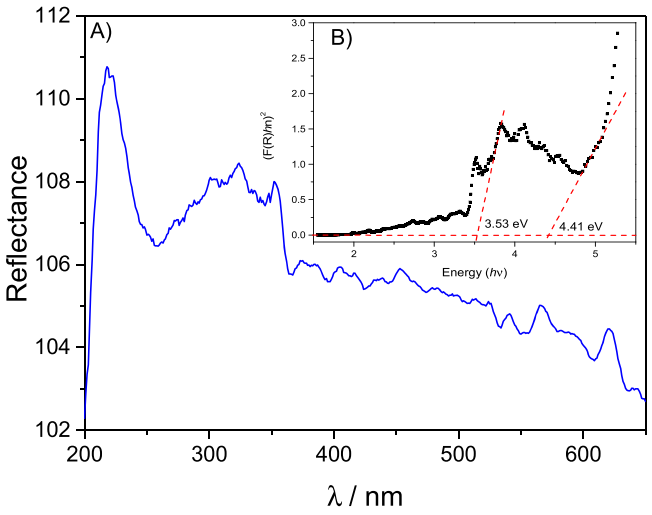

Fig. 6. (A) UV-Vis reflectance spectra of the hybrid nanostructure *Gr/h-BNNs*, showing the absorption edge at 218 nm corresponding to an optical band gap 4.41 eV, and the weak absorption edge at 3.53 eV due to an intermediate nanostructure formed by stacking layers of *h*-Bn and graphene. (B) The optical band gap energy spectrum.

Authors contributions

Paulo V.R. Gomes: Preparation, execution of Raman; planning and execution research. **Nathalia F.B. Azeredo:** Preparation and execution of XRD specifically writing the initial draft. **Luis M.S. Garcia:** Preparation, creation and presentation of the published work. **Giovanni R. Morselli:** Preparation, execution, obtaining of optical properties. **Rômulo A. Ando:** discussion of photocatalysis experiments. **Priscilla J. Zambiazzi:** Preparation, execution and discussion of Raman and discussion of TEM experiments. **Larissa O.Tubo:** Execution of TEM experiments. **Dolores R.R. Lazar:** Preparation, creation and presentation of the published work writing the finally draft. **R.F.B. de Souza:** Management and coordination for the research activity planning and execution. **Debora F. Rodrigues:** works writing the finally draft. **Almir Oliveira Neto:** Oversight and leadership responsibility for the research activity planning and execution.

Declaration of Competing Interest

The authors declare that they have no known competing financial interests or personal relationships that could have appeared to influence the work reported in this paper.

Data availability

No data was used for the research described in the article.

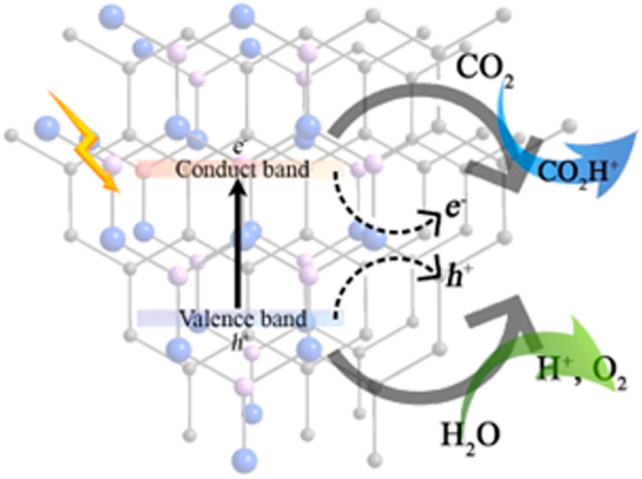

Fig. 8. Schematic pathway of CO_2 photoreduction reaction on Gr/hBNNs material.

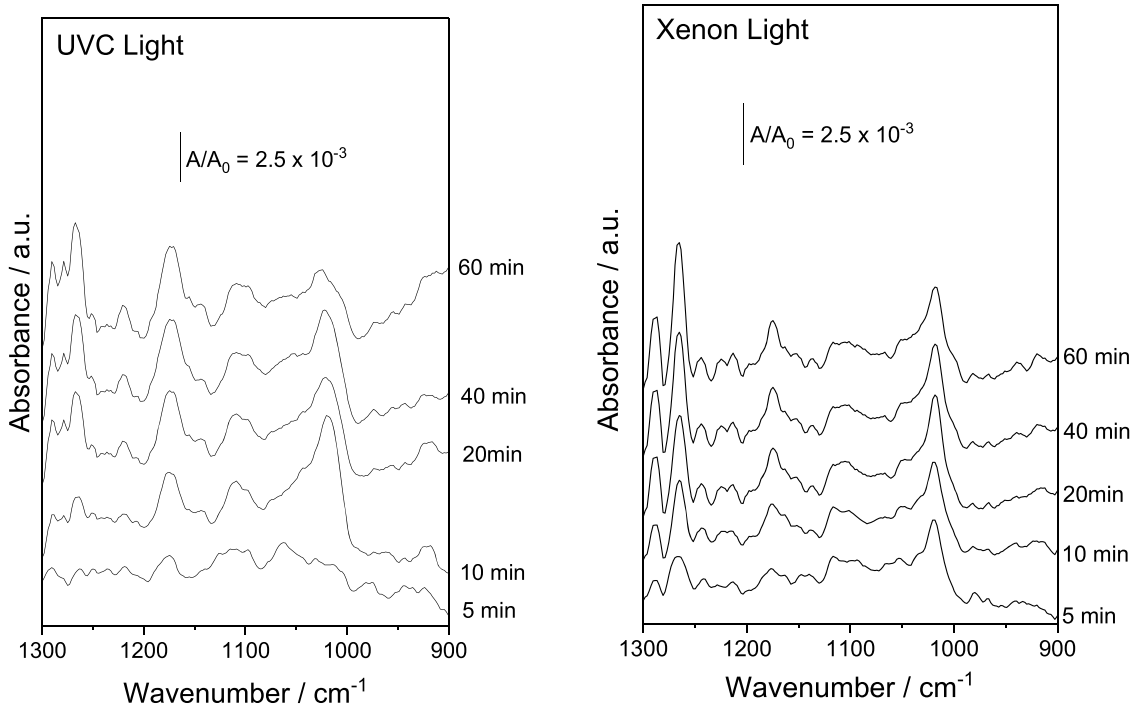

Fig. 7. FTIR spectra were taken from aliquot at 60 min under (a) UVC and (b) white light.

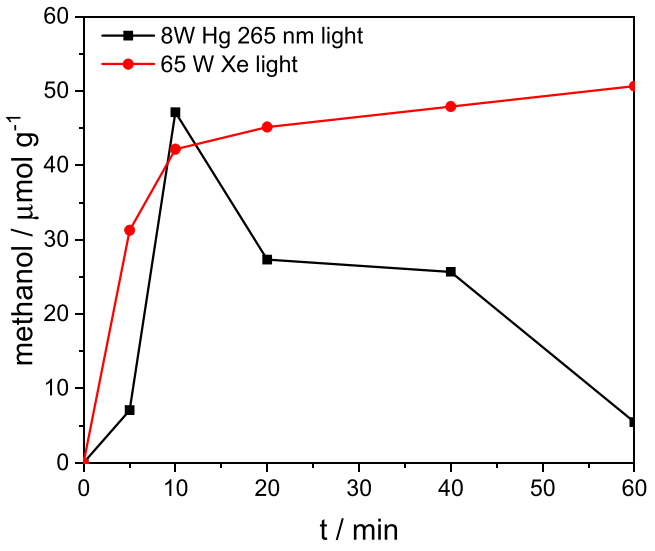

Fig. 9. Time dependence on the methanol yields.

Acknowledgment

We are grateful to CAPES, CNPq (302709/2020-7), FAPESP (2017/11937-4) and CINE-SHELL (ANP)/FAPESP grants 2017/11937-4 for financial supports.

References

[1] J. Li, X. Liu, Y. Feng, J. Yin, Recent progress in polymer/two-dimensional nanosheets composites with novel performances, Prog. Polym. Sci. 126 (2022), 101505, https://doi.org/10.1016/j.progpolymsci.2022.101505.
[2] S. Rana, V. Singh, B. Singh, Recent trends in 2D materials and their polymer composites for effectively harnessing mechanical energy, iScience 25 (2) (2022), 103748, https://doi.org/10.1016/j.isci.2022.103748.
[3] M. Yankowitz, J. Xue, B.J. LeRoy, Graphene on hexagonal boron nitride, J. Phys. Condens. Matter 26 (30) (2014), 303201.10.1088/0953-8984/26/30/303201.
[4] L. Ju, J. Velasco, E. Huang, S. Kahn, C. Nosiglia, H.Z. Tsai, W. Yang, T. Taniguchi, K. Watanabe, Y. Zhang, G. Zhang, M. Crommie, A. Zettl, F. Wang, Photoinduced doping in heterostructures of graphene and boron nitride, Nat. Nanotechnol. 9 (5) (2014) 348–352, https://doi.org/10.1038/nnano.2014.60.
[5] X. Cui, P. Ding, N. Zhuang, L. Shi, N. Song, S. Tang, Thermal conductive and mechanical properties of polymeric composites based on solution-exfoliated boron nitride and graphene nanosheets: a morphology-promoted synergistic effect, ACS Appl. Mater. Interfaces 7 (34) (2015) 19068–19075, https://doi.org/10.1021/acsami.5b04444.
[6] M. Yu, X. Yuan, J. Guo, N. Tang, S. Ye, J. Liang, L. Jiang, Selective graphene-like metal-free 2D nanomaterials and their composites for photocatalysis, Chemosphere 284 (2021), 131254, https://doi.org/10.1016/j.chemosphere.2021.131254.
[7] S. Naghdi, B. Jaleh, M. Eslamipanah, A. Moradi, M. Abdollahi, N. Einali, K.Y. Rhee, Graphene family, and their hybrid structures for electromagnetic interference shielding applications: recent trends and prospects, J. Alloys Compd. 900 (2022), 163176, https://doi.org/10.1016/j.jallcom.2021.163176.
[8] S. Qiu, Y. Hou, W. Xing, C. Ma, X. Zhou, L. Liu, Y. Kan, R.K.K. Yuen, Y. Hu, Self-assembled supermolecular aggregate supported on boron nitride nanoplatelets for flame retardant and friction application, Chem. Eng. J. 349 (2018) 223–234, https://doi.org/10.1016/j.cej.2018.05.053.
[9] S. Singal, A. Joshi, A.K. Tomar, V. Sahu, G. Singh, R.K. Sharma, Vacancies and edges: Enhancing supercapacitive performance metrics of electrode materials, J. Energy Storage 31 (2020), 101614, https://doi.org/10.1016/j.est.2020.101614.
[10] W.W. Dong, J. Jia, Y. Wang, J.R. An, O.Y. Yang, X.J. Gao, Y.L. Liu, J. Zhao, D.S. Li, Visible-light-driven solvent-free photocatalytic CO_2 reduction to CO by Co-MOF/Cu_2O heterojunction with superior selectivity, Chem. Eng. J. 438 (2022), 135622, https://doi.org/10.1016/j.cej.2022.135622.
[11] X. Liu, T. Chen, Y. Xue, J. Fan, S. Shen, M.S.A. Hossain, M.A. Amin, L. Pan, X. Xu, Y. Yamauchi, Nanoarchitectonics of MXene/semiconductor heterojunctions toward artificial photosynthesis via photocatalytic CO_2 reduction, Coord. Chem. Rev. 459 (2022), 214440, https://doi.org/10.1016/j.ccr.2022.214440.
[12] J.F.D. Brito, G.G. Bessegato, J.A.L. Perini, L.D.D.M. Torquato, M.V.B. Zanoni, Advances in photoelectroreduction of CO_2 to hydrocarbons fuels: contributions of functional materials, J. CO2 Util. 55 (2022), 101810, https://doi.org/10.1016/j.jcou.2021.101810.
[13] H. Ma, Y. He, P. Chen, H. Wang, Y. Sun, J. Li, F. Dong, G. Xie, J. Sheng, Ultrathin two-dimensional Bi-based photocatalysts: synthetic strategies, surface defects, and reaction mechanisms, Chem. Eng. J. 417 (2021), 129305, https://doi.org/10.1016/j.cej.2021.129305.
[14] R.F.B. de Souza, V.A. Maia, P.J. Zambiazzi, L. Otubo, D.R.R. Lazar, A.O. Neto, Facile, clean and rapid exfoliation of boron-nitride using a non-thermal plasma process, Mater. Today Adv. 12 (2021), 100181, https://doi.org/10.1016/j.mtadv.2021.100181.
[15] M. Yovanovich, A.J. da Silva, R.F. de Souza, V. Ussui, A.O. Neto, D.R. Lazar, Conversion of methane to methanol using WO_3/TiO_2 porous photocatalyst, Int. J. Electrochem. Sci. 16 (7) (2021), 210735.10.20964/2021.07.65.
[16] M.C.L. Santos, L.C. Nunes, L.M.G. Silva, A.S. Ramos, F.C. Fonseca, R.F.B. de Souza, A.O. Neto, Direct Alkaline anion exchange membrane fuel cell to converting methane into methanol, ChemistrySelect 4 (39) (2019) 11430–11434, https://doi.org/10.1002/slct.201902421.
[17] I.H. Boyaci, H.E. Genis, B. Guven, U. Tamer, N. Alper, A novel method for quantification of ethanol and methanol in distilled alcoholic beverages using Raman spectroscopy, J. Raman Spectrosc. 43 (8) (2012) 1171–1176, https://doi.org/10.1002/jrs.3159.
[18] W. Zhu, X. Gao, Q. Li, H. Li, Y. Chao, M. Li, S.M. Mahurin, H. Li, H. Zhu, S. Dai, Controlled gas exfoliation of boron nitride into few-layered nanosheets, Angew. Chem. Int. Ed. 55 (36) (2016) 10766–10770, https://doi.org/10.1002/anie.201605515.
[19] Y. Wu, B. Wang, Y. Ma, Y. Huang, N. Li, F. Zhang, Y. Chen, Efficient and large-scale synthesis of few-layered graphene using an arc-discharge method and conductivity studies of the resulting films, Nano Res. 3 (9) (2010) 661–669, https://doi.org/10.1007/s12274-010-0027-3.
[20] V. Štengl, J. Henych, M. Slušná, P. Ecorchard, Ultrasound exfoliation of inorganic analogues of graphene, Nanoscale Res. Lett. 9 (1) (2014), 167.10.1186/1556-276x-9-167.
[21] R.V. Gorbachev, I. Riaz, R.R. Nair, R. Jalil, L. Britnell, B.D. Belle, E.W. Hill, K. S. Novoselov, K. Watanabe, T. Taniguchi, A.K. Geim, P. Blake, Hunting for monolayer boron nitride: optical and raman signatures, Small 7 (4) (2011) 465–468, https://doi.org/10.1002/smll.201001628.
[22] J. Shang, F. Xue, C. Fan, E. Ding, Preparation of few layers hexagonal boron nitride nanosheets via high-pressure homogenization, Mater. Lett. 181 (2016) 144–147, https://doi.org/10.1016/j.matlet.2016.05.154.
[23] Z. Lu, C. Wang, X. Chen, M. Song, W. Xia, Effects of buffer gas on N-doped graphene in a non-thermal plasma process, Diamond Relat. Mater. 118 (2021), 108548, https://doi.org/10.1016/j.diamond.2021.108548.
[24] A.C. Ferrari, D.M. Basko, Raman spectroscopy as a versatile tool for studying the properties of graphene, Nat. Nanotechnol. 8 (4) (2013) 235–246, https://doi.org/10.1038/nnano.2013.46.
[25] A. Eckmann, A. Felten, A. Mishchenko, L. Britnell, R. Krupke, K.S. Novoselov, C. Casiraghi, Probing the nature of defects in graphene by Raman spectroscopy, Nano Lett. 12 (8) (2012), 3925-3930.10.1021/nl300901a.
[26] Z.L. Cheng, Z.S. Ma, H.L. Ding, Z. Liu, Environmentally friendly, scalable exfoliation for few-layered hexagonal boron nitride nanosheets (BNNSs) by multi-time thermal expansion based on released gases, J. Mater. Chem. C 7 (46) (2019), 14701-14708.10.1039/C9TC03985F.
[27] R. Jerome, A.K. Sundramoorthy, Preparation of hexagonal boron nitride doped graphene film modified sensor for selective electrochemical detection of nicotine in tobacco sample, Anal. Chim. Acta 1132 (2020) 110–120, https://doi.org/10.1016/j.aca.2020.07.060.
[28] M. Li, M. Wang, X. Hou, Z. Zhan, H. Wang, H. Fu, C.T. Lin, L. Fu, N. Jiang, J. Yu, Highly thermal conductive and electrical insulating polymer composites with boron nitride, Compos. B Eng. 184 (2020), 107746, https://doi.org/10.1016/j.compositesb.2020.107746.
[29] W. Cai, D. Zhang, B. Wang, Y. Shi, Y. Pan, J. Wang, W. Hu, Y. Hu, Scalable one-step synthesis of hydroxylated boron nitride nanosheets for obtaining multifunctional polyvinyl alcohol nanocomposite films: multi-azimuth properties improvement, Compos. Sci. Technol. 168 (2018) 74–80, https://doi.org/10.1016/j.compscitech.2018.09.004.
[30] N. Kostoglou, K. Polychronopoulou, C. Rebholz, Thermal and chemical stability of hexagonal boron nitride (h-BN) nanoplatelets, Vacuum 112 (2015) 42–45, https://doi.org/10.1016/j.vacuum.2014.11.009.
[31] G. Gao, W. Gao, E. Cannuccia, J. Taha-Tijerina, L. Balicas, A. Mathkar, T. N. Narayanan, Z. Liu, B.K. Gupta, J. Peng, Y. Yin, A. Rubio, P.M. Ajayan, Artificially stacked atomic layers: toward new van der Waals solids, Nano Lett. 12 (7) (2012) 3518–3525, https://doi.org/10.1021/nl301061b.
[32] C. Huang, C. Chen, M. Zhang, L. Lin, X. Ye, S. Lin, M. Antonietti, X. Wang, Carbon-doped BN nanosheets for metal-free photoredox catalysis, Nat. Commun. 6 (1) (2015), 7698.10.1038/ncomms8698.
[33] L. Ci, L. Song, C. Jin, D. Jariwala, D. Wu, Y. Li, A. Srivastava, Z.F. Wang, K. Storr, L. Balicas, F. Liu, P.M. Ajayan, Atomic layers of hybridized boron nitride and graphene domains, Nat. Mater. 9 (5) (2010) 430–435, https://doi.org/10.1038/nmat2711.
[34] P. Makuła, M. Pacia, W. Macyk, How To Correctly Determine the Band Gap Energy of Modified Semiconductor Photocatalysts Based on UV–Vis Spectra, J. Phys. Chem. Lett. 9 (23) (2018) 6814–6817, https://doi.org/10.1021/acs.jpclett.8b02892.
[35] K. Watanabe, T. Taniguchi, H. Kanda, Direct-bandgap properties and evidence for ultraviolet lasing of hexagonal boron nitride single crystal, Nat. Mater. 3 (6) (2004) 404–409, https://doi.org/10.1038/nmat1134.
[36] C. Kim, F. Dionigi, V. Beermann, X. Wang, T. Möller, P. Strasser, Alloy nanocatalysts for the electrochemical oxygen reduction (ORR) and the direct electrochemical carbon dioxide reduction reaction (CO2RR), Adv. Mater. 31 (31) (2019), 1805617, https://doi.org/10.1002/adma.201805617.

[37] J. Nandenha, R.M. Piasentin, L.M.G. Silva, E.H. Fontes, A.O. Neto, R.F.B. de Souza, Partial oxidation of methane and generation of electricity using a PEMFC, Ionics 25 (10) (2019) 5077–5082, https://doi.org/10.1007/s11581-019-03186-z.
[38] K.Z. Gaca-Zając, B.R. Smith, A. Nordon, A.J. Fletcher, K. Johnston, J. Sefcik, Investigation of IR and Raman spectra of species present in formaldehyde-water-methanol systems, Vib. Spectrosc. 97 (2018) 44–54, https://doi.org/10.1016/j.vibspec.2018.05.001.
[39] J. Nandenha, I. Nagahama, J. Yamashita, E. Fontes, J. Ayoub, R. de Souza, F. Fonseca, A. Neto, Activation of methane on PdZn/C electrocatalysts in an acidic electrolyte at low temperatures, Int. J. Electrochem. Sci. 14 (2019) 10819–10834.
[40] E. Karamian, S. Sharifnia, On the general mechanism of photocatalytic reduction of CO_2, J. CO2 Util. 16 (2016) 194–203, https://doi.org/10.1016/j.jcou.2016.07.004.
[41] C. Zhou, C. Lai, C. Zhang, G. Zeng, D. Huang, M. Cheng, L. Hu, W. Xiong, M. Chen, J. Wang, Y. Yang, L. Jiang, Semiconductor/boron nitride composites: synthesis, properties, and photocatalysis applications, Appl. Catal. B 238 (2018) 6–18, https://doi.org/10.1016/j.apcatb.2018.07.011.
[42] A. Kumar, V. Hasija, A. Sudhaik, P. Raizada, Q. Van Le, P. Singh, T.H. Pham, T. Kim, S. Ghotekar, V.H. Nguyen, Artificial leaf for light-driven CO_2 reduction: basic concepts, advanced structures and selective solar-to-chemical products, Chem. Eng. J. 430 (2022), 133031, https://doi.org/10.1016/j.cej.2021.133031.
[43] W. Tu, Y. Zhou, Z. Zou, Photocatalytic conversion of CO_2 into renewable hydrocarbon fuels: state-of-the-art accomplishment, challenges, and prospects, Adv. Mater. 26 (27) (2014) 4607–4626, https://doi.org/10.1002/adma.201400087.